Electrochimica Acta 260 (2018) 348–357

Contents lists available at ScienceDirect

Electrochimica Acta

journal homepage: www.elsevier.com/locate/electacta

Linking the Cu(II/I) potential to the onset of dynamic phenomena at corroding copper microelectrodes immersed in aqueous 0.5 M NaCl

Amelia Rose Langley [a], Mariolino Carta [b], Richard Malpass-Evans [b], Neil B. McKeown [b], Jonathan H.P. Dawes [c], Ellen Murphy [c], Frank Marken [a, *]

[a] Department of Chemistry, University of Bath, Claverton Down, Bath, BA2 7AY, UK
[b] School of Chemistry, University of Edinburgh, Joseph Black Building, West Mains Road, Edinburgh, Scotland, EH9 3JJ, UK
[c] Bath Institute for Mathematical Innovation, University of Bath, Claverton Down, BA2 7AY, UK

ARTICLE INFO

Article history:
Received 22 September 2017
Received in revised form
11 December 2017
Accepted 11 December 2017
Available online 14 December 2017

Keywords:
Copper
Alloy
Oxygen
Seawater
Chaos
Colloid

ABSTRACT

Electrochemical studies have been conducted at copper microelectrodes (125, 50, and 25 μm in diameter) immersed in aqueous 0.5 M NaCl. Cyclic and linear sweep voltammetry were used to explore the corrosion of copper in chloride media. Cyclic voltammetry revealed the reversible Cu(I)/Cu(0) potential at approximately −0.11 V vs. SCE associated with the formation of a dense CuCl blocking layer (confirmed by *in situ* Raman and fluorescence measurements). Although continuous dissolution of Cu(I) occurs, only an increase in the driving potential into the region of the Cu(II)/Cu(I) potential at approximately +0.14 V vs. SCE started more rapid and stochastic dissolution/corrosion processes. The corrosion process is demonstrated to be linked to two distinct mechanisms based on (A) slow molecular dissolution and (B) fast colloidal dissolution. A polymer of intrinsic microporosity (PIM-EA-TB) is employed to suppress colloidal processes to reveal the underlying molecular processes.

1. Introduction

Corrosion is a dynamic process, which is understood as a natural conversion of a metal/alloy to a more stable form, such as metal oxides (atmospheric) and metal chlorides (marine). Corrosion is an extremely dynamic process, which occurs in a range of environments, affecting the properties and integrity of metals. A commonly used metal, due to its high conductivity, is copper which in fact has considerable resistance to atmospheric corrosion [1], compared to that of corrosion in aquatic marine environments [2].

The corrosion of copper in the aquatic environment is chemically complex and not always well understood. The variables that affect copper corrosion in such environments, include temperature [3], pH [4], salt concentration [2,4], and microbiological activity [5], which makes the process difficult to model and understand, both mathematically and electrochemically. In some cases it has been observed that metals, including copper, show oscillatory electrochemical behavior [6]. For copper in acidic chloride containing media oscillatory phenomena have been observed by Lee et al. [7]. These oscillations have fundamentally been assigned to the formation of chloride films "blocking" and "unblocking" current flow. There have been attempts for example by Pearlstein et al. [8] at mathematically modelling the experimental current oscillations observed for copper at a rotating disk electrode. Fundamentally, two competing processes were considered based on CuCl film growth (equation (1)) and dissolution (equation (2)).

$$Cu(s) + Cl^-(aq) \rightleftarrows CuCl(s) + e^- \quad (1)$$

$$CuCl(s) + Cl^-(aq) \rightleftarrows CuCl_2^-(aq) \quad (2)$$

CuCl growth slowing down for thicker films and dissolution causing localized thinning has been suggested to lead to instability and, under the right conditions, to oscillatory phenomena. However, the possible role of Cu(II) in this reaction sequence deserves further attention. In work by Crundwell [9] Cu^{2+} was detected during copper corrosion in hydrochloric acid and it was pointed out that the role of Cu^{2+} is not well understood. Itagaki and coworkers [10] demonstrated with elegant channel flow double electrode experiments in aqueous sulfuric acid/NaCl solution that the rate of formation of Cu^{2+} sympathized with the rate of corrosion (or copper oxidation) even in chaotic current oscillation regimes. More

* Corresponding author.
E-mail address: f.marken@bath.ac.uk (F. Marken).

https://doi.org/10.1016/j.electacta.2017.12.083
0013-4686/

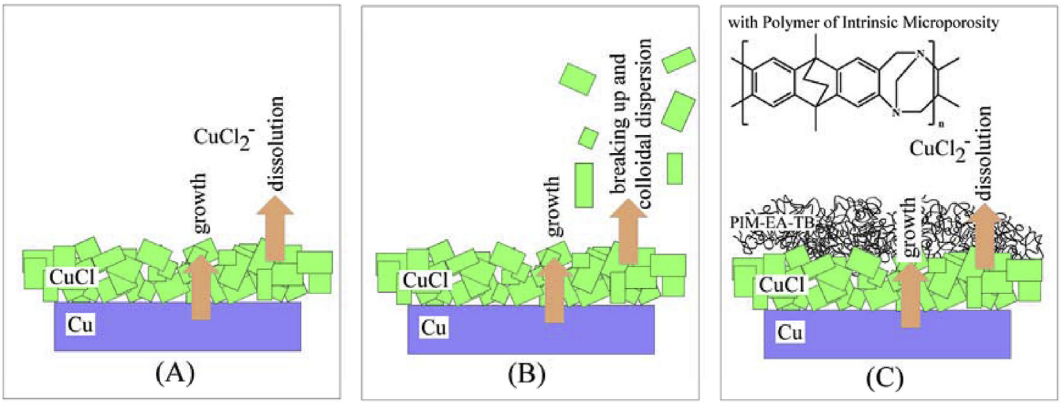

Fig. 1. Graphical illustration of (A) the CuCl precipitation-dissolution mechanism suggested to be responsible for oscillatory behavior in acidified chloride media, (B) the redox driven Cu(II)/Cu(I) destabilization of CuCl observed in neutral chloride media associated with colloidal break-up of the CuCl film, and (C) the process when investigated under a coating of PIM-EA-TB to prevent colloidal break-up.

recent work has been reported also on copper electro-dissolution in a micro-fluidic chip in aqueous phosphoric acid [11]. The mechanism is revisited here for the case of copper in neutral aqueous 0.5 M NaCl (model sea water) and for microelectrodes [12] rather than under hydrodynamic rotating disk conditions. Microelectrodes offer conditions (i) consistent with well-defined diffusional flux (similar to hydrodynamic experiments [13]), but also (ii) related to the environment where a pore in a cable insulation is the cause for copper corrosion.

Fig. 1 shows a schematic drawing of the copper | electrolyte interface when exposed to aqueous chloride solution. Either from oxidizing species in solution or via externally applied potential, the copper oxidation can be driven to give a CuCl ($K_{SP} = 1.72 \times 10^{-7}$ M^2 at 25 °C [14]) surface deposit. It is well known that particularly excess chloride in solution can lead to more soluble chloro-cuprate(I) species [15] and that continuous dissolution occurs depending on the concentration of aqueous chloride. Fig. 1A describes the case of CuCl growth competing with CuCl dissolution. This process has been suggested to be primarily responsible for oscillatory phenomena. Fig. 1B schematically shows a process in which colloidal particles are released into the aqueous solution; a process driven by mechanical destabilization of the CuCl film coating as shown in this report. Fig. 1C illustrates the idea of placing an intrinsically microporous polymer film, PIM-EA-TB, over the copper surface to stop the colloidal mechanism whilst still allowing dissolution of molecular chloro-cuprates(I).

Polymers of intrinsic microporosity (PIMs) have been developed over the past decade [16] as a class of molecularly defined highly rigid structures with the ability to bind [17] and separate [18] gases. PIMs have been introduced to electrochemistry only recently [19] with potential applications in the stabilization of fuel cell catalysts [20] or the protection of nanoparticle catalysts [21]. The structure of PIM-EA-TB is shown in Fig. 1C and is based on an ethanoanthracene unit ("EA") as well as a Tröger base unit ("TB") [22]. One unique benefit of PIM materials such as PIM-EA-TB is their processability. Films and coatings are readily formed from chloroform solution [23]. Here PIM-EA-TB is applied to a copper microelectrode surface to separate "molecular mechanisms" and "colloidal mechanisms". The microporous polymer allows transport of molecules and ions but suppresses the transport of particulate species.

In this report copper microelectrode reactivity is studied for 25 μm, 50 μm, and 125 μm diameter electrodes immersed in aqueous 0.5 M NaCl. These conditions mimic marine conditions and are therefore relevant in processes involving copper equipment subsea. It is shown that stochastic current responses are associated not only with Cu(I) formation, but also with Cu(II) formation. It is suggested that Cu(II) destabilizes the CuCl blocking layer and thereby initiates stochastic and oscillatory phenomena.

2. Experimental

2.1. Chemical reagents

For the preparation of aqueous electrolytes NaCl (≥99.8% purity), $Cu(II)Cl_2$ (99.999% purity) and H_2SO_4 (ACS reagent, 1.84 g mL^{-1}) were used. All electrolytes were made using deionized water (18.2 MΩ cm, CE Instruments Ltd.). Reference copper chloride compounds, Cu(I)Cl (anhydrous, ≥ 99.99% purity, Sigma-Aldrich) and $Cu(II)Cl_2$ (99.999% purity, Sigma Aldrich) were used as reference materials for Raman spectroscopy experiments.

2.2. Electrochemical measurements

All electrochemical measurements were conducted in aqueous 0.5 M NaCl electrolyte solution at 20 ± 2 °C. A three-electrode configuration was employed, consisting of the copper working microelectrode, a KCl-saturated calomel reference electrode (SCE), and a platinum wire counter electrode, connected to a micro-Autolab III potentiostat (Ecochemie, Netherlands) with GPES software.

2.3. Fabrication of copper microelectrodes

Three copper microelectrodes were constructed for electrochemical investigation of diameters 25 μm, 50 μm, and 125 μm. The microelectrodes were assembled by threading copper wire (ADVENT UK, 99.90% purity) through a glass tube which is then immobilized by a non-conducting transparent epoxy resin (PRESI MA2; 10:1 ratio MECAPREX resin:triethylenetetramine). The microelectrodes were placed in an oven at 100 °C for approximately 2 h for the resin to set and cure. The microelectrodes were subsequently polished, and electrical contact was ensured using copper conducting tape (3 M). Electrodes were investigated with scanning electron microscopy (SEM, JEOL SEM6480LV). Images shown in Fig. 2 allowed for microelectrode size calibration.

2.4. In situ Raman and fluorescence measurements

In situ Raman spectroscopy (Renishaw's inVia confocal Raman

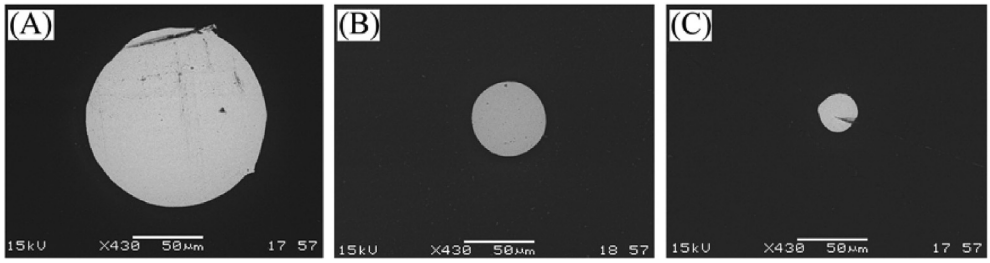

Fig. 2. SEM images of polished copper microelectrodes of diameters (A) 125 µm, (B) 50 µm, and (C) 25 µm before use.

microscope) was used to investigate surface material changes during the anodic polarization of a 125 µm diameter copper working microelectrode. The electrochemical cell consisted of Pt wire counter and reference electrodes. In aqueous 0.5 M NaCl the Pt wire pseudo reference electrode provides a potential 400 mV negative of the SCE reference potential. *In situ* Raman experiments were carried out with a beam intensity of 10% (532 nm) between 60 and 1800 cm^{-1}. The electrochemical cell was connected to a microAutolab III potentiostat (Ecochemie, Netherlands) with GPES software. Raman spectra were collected every 5 s during linear sweep voltammetry from −0.6 V to +5.0 V *vs.* Pt (corresponding to −0.2 V to 5.4 V *vs.* SCE) at 20 mV s^{-1} in 0.5 M NaCl. Reference Raman spectra for Cu(I)Cl and Cu(II)Cl_2 on glass slides were taken with beam intensities of 1.0% and 0.1% (532 nm) respectively, where $CuCl_2$ would degrade due to heat at 1% beam intensity. Spectra were taken between 100 and 4000 cm^{-1}.

3. Results and discussion

3.1. The Cu(I/0) surface redox process in aqueous 0.5 M NaCl

Initially, only the first redox process associated with the formation of CuCl is investigated. Fig. 3 shows cyclic voltammetry data for copper microelectrodes (diameter 25 µm, 50 µm, and 125 µm) immersed in aqueous 0.5 M NaCl. An oxidation peak occurs associated with the oxidation from Cu(0) to Cu(I) and during the reverse potential sweep, the Cu(I/0) reduction peak is observed. Data for peak position and charge are summarised in Table 1. A plot of logarithm of current *versus* potential is shown in the inset in Fig. 3A to illustrate the fact that two mechanisms are observed in separate potential domains. In the initial potential range up to *ca.* −0.1 V *vs.* SCE a linear slope with close to 59 mV (Nernstian) gradient suggests reversible conditions with Cu(I) being formed and dissolved reversibly into the chloride containing electrolyte (equation (3)). At approximately −0.1 V *vs.* SCE an abrupt change in slope indicates nucleation of a new solid, CuCl (equation (4)), which then grows over the electrode surface to block the surface and in part suppress dissolution. A similar peak is observed for the reduction (when scanning the potential into negative direction), but only for faster scan rates. At a slow scan rate of 1 mV s^{-1} the reduction peak is not observed. The reason for this observation is a constant flux/dissolution of Cu(I) away from the electrode into the solution due to partial solubility ($K_{SP} = 1.72 \times 10^{-7}$ M^2 at 25 °C [14], which is further affected by the presence of excess chloride [24]).

$$Cu(s) + 2\,Cl^-(aq) \rightleftarrows Cu(I)Cl_2^-(aq) + e^- \quad (3)$$

$$Cu(s) + Cl^-(aq) \rightleftarrows CuCl(s) + e^- \quad (4)$$

Analysis of the peak position for oxidation and for the reduction allows an approximate midpoint potential $E_{mid} = ½ (E_p^{ox} + E_p^{red}) = -0.11$ V *vs.* SCE to be estimated, but this value is scan rate dependent and affected by nucleation and dissolution processes. Peak currents show scan rate dependence, which is most obvious in the ratio I_p^{red}/I_p^{ox} (see Table 1), which approaches zero for slower scan rates and for smaller microelectrodes (probably due to CuCl dissolution driven by diffusion). The charge under the oxidation peak also is scan rate dependent as shown in Fig. 3D. At lower scan rate the charge increases due to the concomitant dissolution. At faster scan rate the charge under the oxidation peak roughly scales with the electrode area (see Table 1) indicative of a film of CuCl with approximately 0.16 C cm^{-2}. With a typical density for CuCl of 4.139 g cm^{-3} [25] this suggests an estimated thickness of approximately 0.4 µm.

The presence of CuCl is confirmed by *in situ* Raman and fluorescence data. Fig. 4A shows Raman spectra for CuCl and $CuCl_2$ reference materials with a strong fluorescence signal only for CuCl and distinct vibrational bands for $CuCl_2$. When performing the copper voltammetry experiment with a 125 µm diameter copper electrode (inverted) and the Raman microscope focused onto the corroding surface, the strong fluorescence signal for CuCl is immediately observed (Fig. 4B). Vibrational bands at 150 cm^{-1} confirm the presence of CuCl. In the first 10 s (corresponding to reaching 0.0 V vs. SCE) of the corrosion process the CuCl signal can be seen to increase. During more prolonged anodic corrosion at higher applied potentials the fluorescence signal decreases again (not shown), which is likely to be linked to loss of focus (due to recess formation) rather than loss of CuCl. The formation of other side products and in particular Cu(II) is still possible due to *in situ* Raman not being very sensitive under these conditions.

3.2. The Cu(II/I) surface redox process in aqueous 0.5 M NaCl

When expanding the potential window positively, more complex behaviour for the copper oxidation in aqueous 0.5 M NaCl (here employed as model sea water) is observed. Fig. 5 shows typical voltammetric features for copper microelectrodes of 25 µm, 50 µm, and 125 µm diameter. A second oxidation signal appears at a potential positive of 0.0 V *vs.* SCE. Peak features are observed for 125 µm diameter electrodes, but for smaller electrodes only an onset of noise occurs at 0.1 V *vs.* SCE. The noise signal is accompanied by a higher level of anodic current (average) indicative of more rapid corrosion and loss of Cu into the solution. It is interesting to compare the onset of current noise with the oxidation of Cu(I) to Cu(II) in aqueous 0.5 M NaCl. Data in Fig. 5D show a superposition of the copper corrosion signal with a solution phase voltammogram for 10 mM $CuCl_2$ dissolved in 0.5 M NaCl at a glassy carbon electrode. The formation of Cu(II) in solution with $E_{mid} = 0.14$ V *vs.* SCE (consistent with literature [26]; equation (5)) appears to be linked to the onset of noise at the copper electrode. This potential is also linked to the point during the negative going scan (see Fig. 5D) where the stochastic current noise seizes. It is interesting to further explore the origin of the current noise. The current noise is associated with an (in average) increase in current

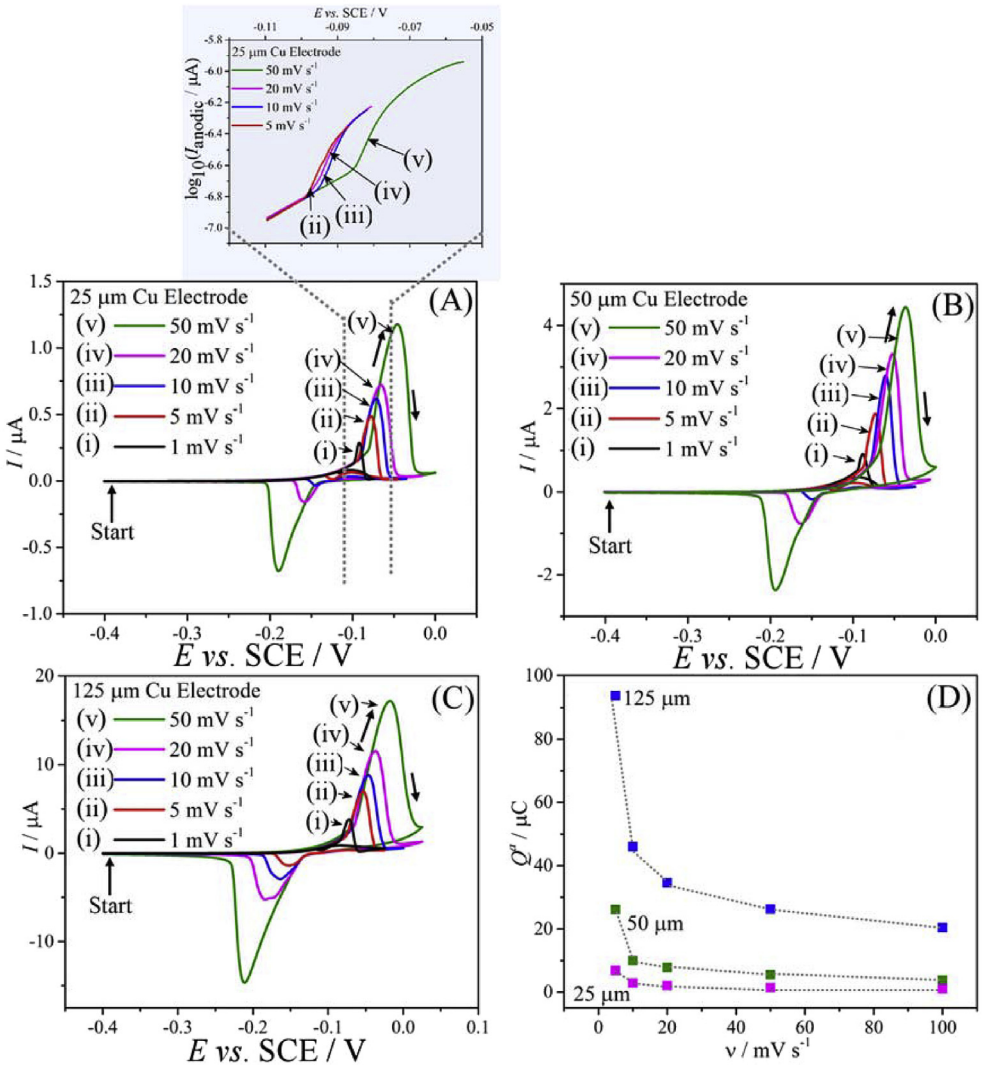

Fig. 3. Cyclic voltammograms at 1, 5, 10, 20 and 50 mV s^{-1} scan rates in 0.5 M NaCl(aq) for (A) 25 µm, (B) 50 µm, and (C) 125 µm diameter (epoxy-mounted) copper electrodes. A plot of anodic charge, Q^{ox} versus scan rate (ν) is given for each electrode size.

and therefore an increase in Cu dissolution. This suggests that an additional mechanism is in operation to increase the rate of dissolution/corrosion.

Table 1
Summary of data from cyclic voltammograms in Fig. 3 for 25, 50 and 125 µm diameter Cu microelectrodes immersed in 0.5 M NaCl.

ø/µm	ν/mV s^{-1}	I_p^{ox}/µA	I_p^{red}/µA	Q^{ox}/µC	I_p^{red}/I_p^{ox}	E_p^{ox}/mV	E_p^{red}/mV	ΔE_p/mV
25	50	1.18	−0.68	1.06	0.58	−46	−190	144
	20	0.72	−0.16	1.39	0.22	−65	−158	93
	10	0.61	−0.03	2.00	0.05	−71	−144	73
	5	0.49	n/a	2.84	n/a	−77	−123	46
	1	0.29	n/a	6.82	n/a	−92	n/a	n/a
50	50	4.44	−2.36	3.76	0.53	−36	−193	229
	20	3.31	−0.77	5.52	0.23	−52	−163	111
	10	2.80	−0.18	7.77	0.06	−60	−149	87
	5	1.89	n/a	9.96	n/a	−73	−123	50
	1	0.91	n/a	26.1	n/a	−89	n/a	n/a
125	50	17.2	−14.65	20.4	0.85	−18	−211	193
	20	11.5	−5.24	26.2	0.45	−37	−183	146
	10	8.82	−2.93	34.6	0.33	−46	−164	117
	5	6.97	−1.39	45.9	0.20	−54	−153	99
	1	3.83	n/a	93.7	n/a	−72	n/a	n/a

ø = electrode diameter; ν = scan rate; I_p^{ox} = anodic peak current; I_p^{red} = cathodic peak current; E_p^{ox} = anodic peak potential; E_p^{red} = cathodic peak potential; and ΔE_p = peak potential separation.

$$Cu(I)(aq) \rightleftarrows Cu(II)(aq) + e^- \quad (5)$$

When scanning the potential applied to copper microelectrodes further into the positive potential range (consistent with a higher potential applied to a copper conductor immersed in sea water), the current noise can be observed to continue. It could be suggested that at higher potentials the mechanism should change and water electrolysis should occur, but currents remain reasonably constant and no gas evolution occurs. *In situ* microscopy experiments were performed to further investigate this point, but no evidence for gas formation is apparent even at higher applied voltages. This also suggests that stochastic phenomena in current traces are unlikely to be linked to gas bubble blocking or agitation effects. This behaviour could be linked to the formation of mainly an insulating CuCl film with most of the applied potential dropping across this film, so that at the location of the interfacial electron transfer only a lower potential is present. In Fig. 6A voltammetric data are shown for three different electrode sizes and as a function of the scan rate. For all three electrode sizes substantial current noise is observed. The average current at 5 V *vs.* SCE is 0.3 µA, 2.0 µA, and 8.0 µA for electrodes of 25 µm, 50 µm, and 125 µm diameter, respectively, which suggests an average current approximately scaling with electrode area. However, during the copper oxidation substantial

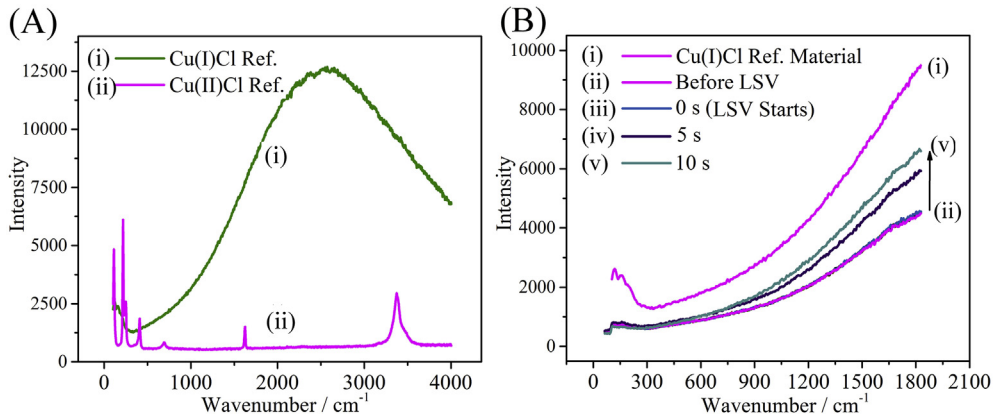

Fig. 4. (A) Raman and fluorescence response for CuCl and $CuCl_2$ reference materials. (B) *In situ* Raman/fluorescence monitoring of the anodic corrosion reaction at a 125 μm diameter copper microelectrode immersed in 0.5 M NaCl(aq) with applied potential scanning (scan rate 20 mVs^{-1}) from −0.2 V to +5.4 V *vs.* SCE to give Raman data sets for every 0.1 V interval (data shown only for data set at (iii) −0.2, (iv) −0.1, (v) and 0.0 V vs. SCE).

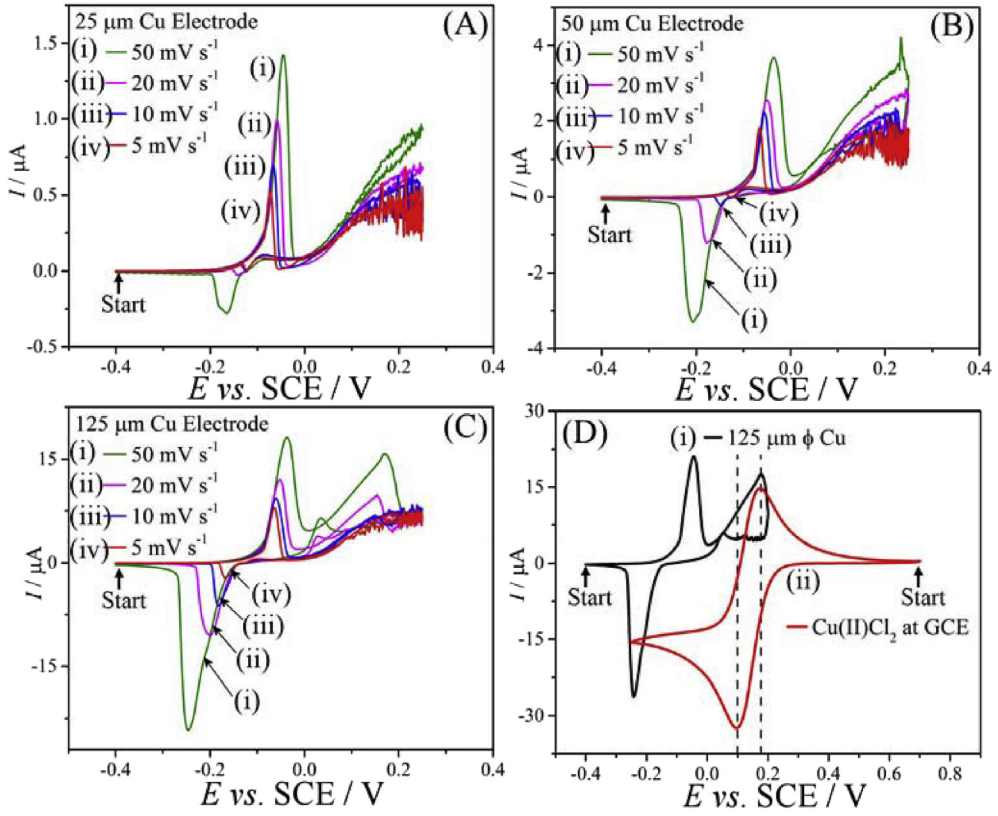

Fig. 5. Cyclic voltammograms (scan rate 50, 20, 10 and 5 mV s^{-1}) starting from −0.30 V to +0.25 V *vs.* SCE for (A) 25, (B) 50, and (C) 125 μm diameter copper microelectrodes immersed in 0.5 M NaCl. (D) Cyclic voltammograms (scan rate 50 mV s^{-1}) comparing at 125 μm diameter copper electrode in 0.5 M NaCl (black) and 3 mm diameter glassy carbon electrode immersed in 10 mM $CuCl_2$ in 0.5 M NaCl (red). (For interpretation of the references to colour in this figure legend, the reader is referred to the Web version of this article.)

loss of copper occurs and the microelectrodes become recessed. This recess formation is obviously a reflection of the progress of the corrosion process through a pore, but also important mechanistically as deeper recess conditions could change the chemical conditions at the corroding surface. Therefore, the voltammetric data are re-plotted in Fig. 6B to show recess development (calculated based on a one-electron process and a Cu density 8.933 g cm^{-3} [27]; reactions leading to products other than Cu(I) are assumed to remain insignificant and capacitive charging currents are anticipated in pA range and therefore ignored here; values have to be considered as estimates as directly measured recession data are not available). Clearly the higher flux of material at the smaller microelectrode is associated with more severe recess formation. For the 25 μm diameter electrode and over the period of the linear sweep potential scan approximately 60 μm recess formation occurs. This compares to only a 40 μm recess at the 125 μm diameter electrode.

An increase in scan rate clearly affects the current data. A noisy anodic peak at approximately +1 V *vs.* SCE is shifted positive upon increasing the scan rate (see Fig. 6C) indicative of a potential-

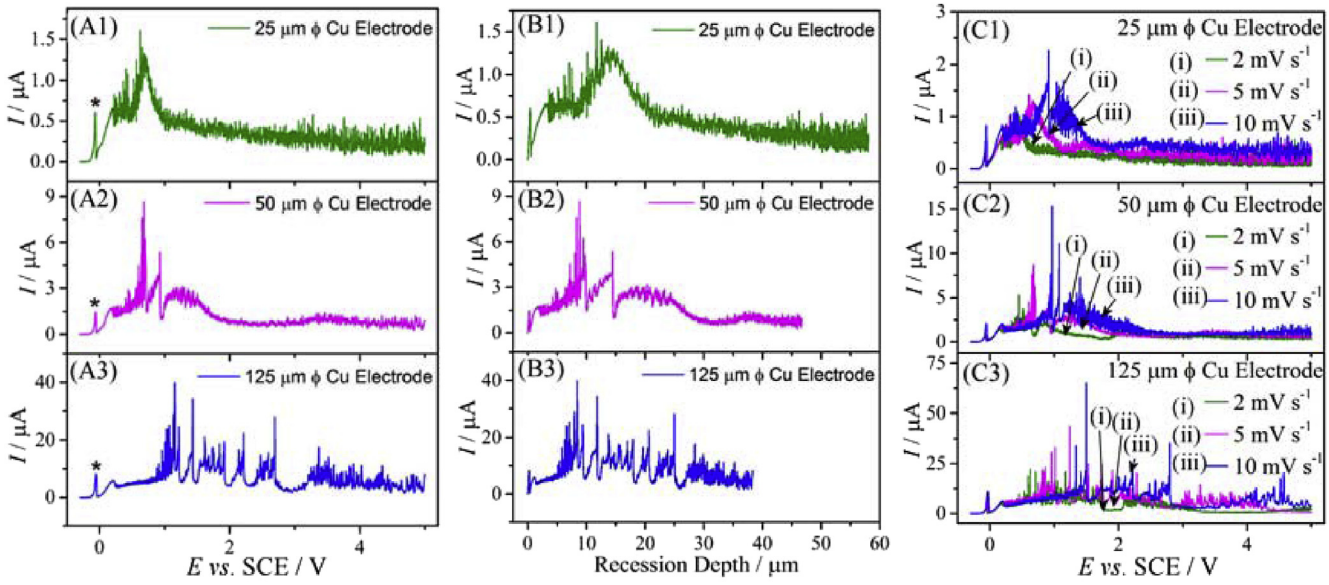

Fig. 6. (A) Linear sweep voltammograms (scan rate 5 mV s^{-1}) from −0.3 to +5.0 V *vs.* SCE at (A1) 25, (A2) 50, and (A3) 125 μm diameter copper microelectrodes immersed in 0.5 M NaCl (the initial Cu(I/0) anodic peak is labelled with an asterisk). (B) As above, but data replotted versus recession depth, which has been estimated based on a copper density of 8.93 g cm^{-3}. (C) As above but for a scan rate of 2, 5, and 10 mV s^{-1}.

independent kinetically controlled process. A region of higher activity appears to be followed by a region of lower activity, although for 125 μm diameter copper electrodes clearly substantial fluctuations occur also at higher potentials. It is possible that the magnitude of the current in this region is to some extent affected by the degree of electrode recession. Further evidence is obtained from electron optical images (Fig. 7).

The scanning electron microscopy (SEM) images indicate conclusively that a film has formed during linear sweep voltammetry to 5 V *vs.* SCE at a scan rate of 5 mV s^{-1} (compare with the SEM images in Fig. 2). The SEM images also show the presence of particulate material on both the electrode and on the resin surrounding the copper microelectrodes. Particulate deposits outside of the electrode perimeter could be an indication of colloidal/particulate material being dislodged from the electrode surface. Elemental analysis based on EDX confirms both Cu and Cl (see Fig. 8). A cube-like morphology is consistent with formation of CuCl [28].

Particulate deposits outside of the electrode perimeter suggest that material has been dislodged after being formed at the electrode surface. Fig. 1B schematically presents the idea of CuCl particles being lost from the electrode surface into the surrounding solution. It appears likely that the onset of stochastic anodic currents could be linked to the formation and expulsion of particulate CuCl. In order to better understand the observed stochastic current fluctuations and the underlying mechanism, further experiments

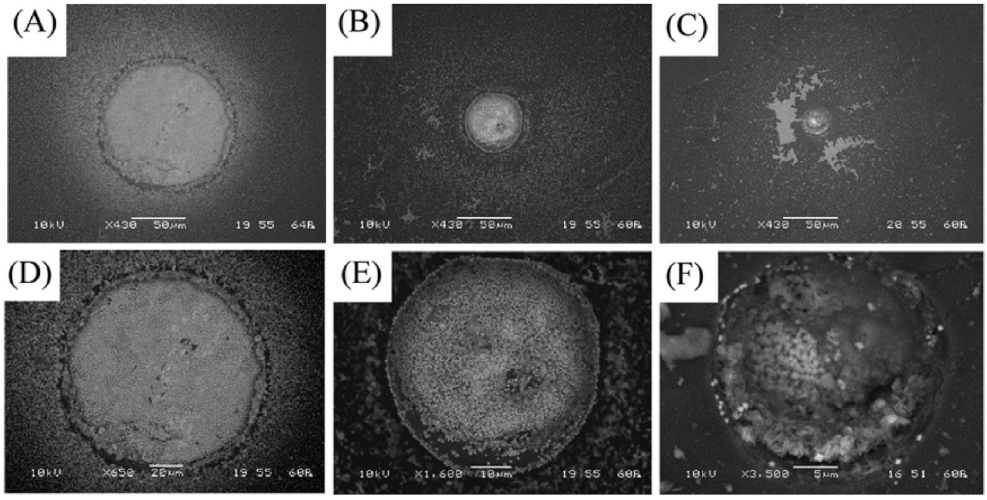

Fig. 7. Scanning electron microscopy (SEM) images for copper microelectrodes of diameters (A,D) 125 μm, (B,E) 50 μm, and (C,F) 25 μm after linear sweep voltammetry from −0.3 V to 5.0 V *vs.* SCE at 5 mV s^{-1}. Images A-C are scaled to images D-F to reveal more details.

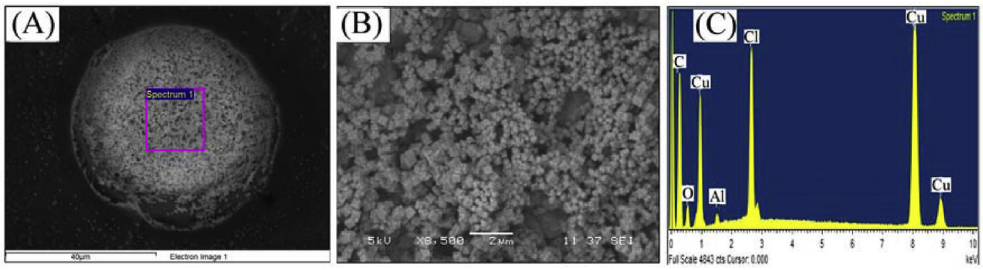

Fig. 8. (A,B) SEM images of the surface of a 50 μm diameter Cu microelectrode after linear sweep voltammetry from −0.3 V to 5.0 V vs. SCE at 5 mV s^{-1} in 0.5 M NaCl. (C) Energy-dispersive X-ray elemental analysis (EDX) for the area indicated in (A).

are conducted with a microporous polymer film (PIM-EA-TB) applied to the electrode surface. The hypothesis in these experiments is based on recent observations that PIM-EA-TB can stop colloidal processes and protect nano-particle deposits whilst allowing molecular processes to proceed.

It is interesting to explore the effect of pH on the corrosion phenomena in particular in order to link the phenomena observed here with those reported previously in the literature. Fig. 9 shows linear sweep voltammetry data obtained at a 50 μm diameter copper microelectrode immersed into 0.5 M NaCl with increasing concentrations of H_2SO_4. It can be seen that even a low concentration of acid strongly enhances the corrosion current, but only after the Cu(II/I) potential region has been reached. Stochastic oscillatory phenomena are seen with 5 mM and 50 mM H_2SO_4. Only with 500 mM H_2SO_4 a new more regular oscillatory process emerges at a potential higher than 4 V *vs.* SCE. This process is likely to be linked to similar processes reported in the literature, although spherical diffusion into a recessed microelectrode is employed rather than hydrodynamic rotating disk electrode methods.

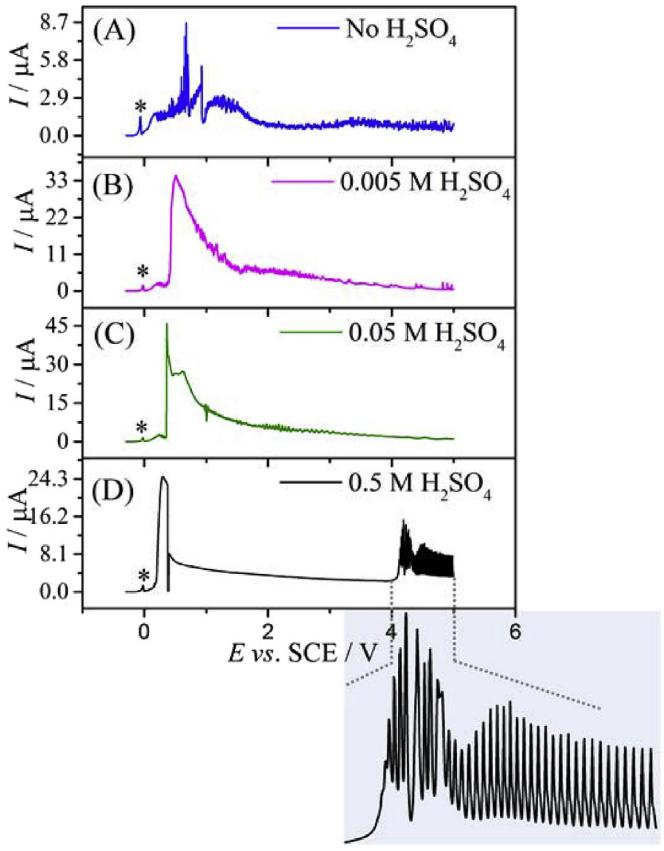

Fig. 9. (A) Linear sweep voltammograms (scan rate 5 mV s^{-1}) from −0.3 to +5.0 V *vs.* SCE at a 50 μm diameter copper microelectrode immersed in 0.5 M NaCl (the initial Cu(I/0) anodic peak is labelled with an asterisk). (B) As above with 5 mM H_2SO_4 added. (C) As above with 50 mM H_2SO_4 added. (D) As above with 500 mM H_2SO_4 added. Inset showing onset of oscillations.

3.3. *Polymer of intrinsic microporosity damping of Cu surface redox processes in aqueous 0.5 M NaCl*

A microporous polymer was introduced to the electrode surface; a polymer of intrinsic microporosity (PIM). After polishing the copper surface, different amounts of PIM-EA-TB in chloroform were applied (1.0, 2.0, 4.0 μg μL^{-1}) via drop-casting (10 μL). Approximate coating thicknesses were calculated using the density of PIM-EA-TB (~1.1 g cm^{-3}), giving 0.5, 0.9 and 1.9 μm for the drop-cast concentrations 1.0, 2.0 and 4.0 μg μL^{-1}, respectively. PIM-EA-TB was chosen based on high intrinsic microporosity with typically 1–2 nm diameter pores [29] and ability for both cations and anions to permeate through the pores [23].

Data in Fig. 10A demonstrates the effect of the PIM-EA-TB coating on the Cu(I/0) redox process. A decrease in both anodic and cathodic current responses can be linked to the slower transport through the microporous polymer film with increasing film thickness thus affecting the rate of copper dissolution. However, the nature of the copper oxidation process remains and the nucleation event leading to the CuCl films deposit formation is evident from the shape of the voltammograms. Effects are less pronounced at the larger 125 μm diameter electrode because mass transport (or flux) is less effective at larger diameter. Although a more complex interaction of copper species with the PIM-EA-TB coating cannot be ruled out, there appears to be in first approximation no significant change in surface corrosion conditions after polymer coating apart from a change in diffusional flux. Data in Fig. 10B shows linear sweep voltammograms comparing bare copper with a 4 μg μL^{-1} PIM-EA-TB deposit. The initial stages of the process including the Cu(I/0) surface redox process remain very similar upon comparison. Only at more positive potential a suppression of the stochastic large current noise is observed (in particular for the 125 μm diameter electrode).

From data in Fig. 10 it can be confirmed that, in addition to the molecular dissolution mechanism, there is a colloidal or particulate mechanism in which loss of CuCl from the electrode surface occurs. The PIM-EA-TB coating can help suppress this loss to some extent. The overall process can be dissected (in a very over-simplified way) into two distinct potential domains (see Fig. 11).

Domain I: At lower applied potential (domain I) the CuCl layer forms and is maintained. This is likely to be associated with formation of Cu(I) at the copper electrode surface coupled to ion

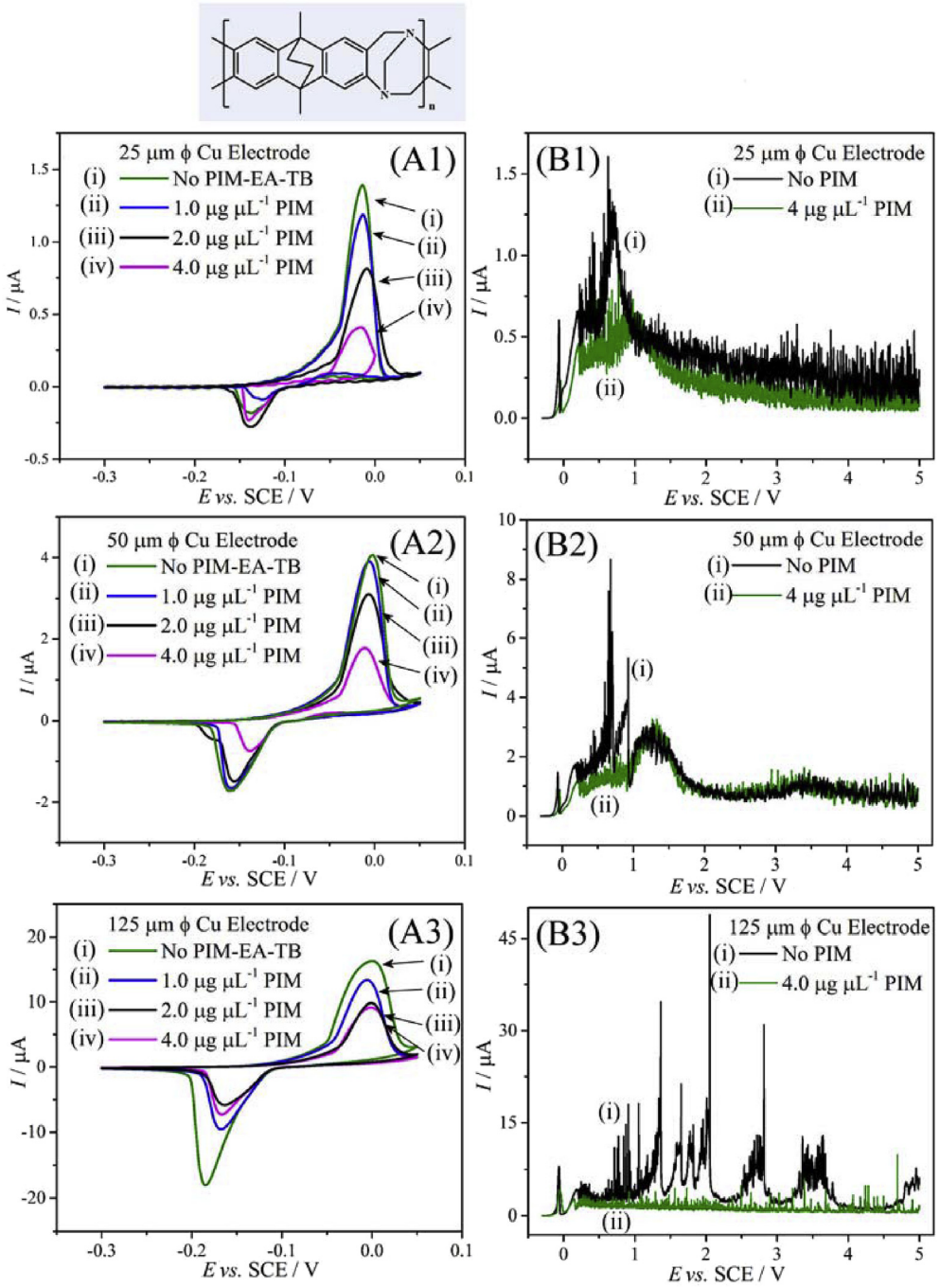

Fig. 10. (A) Cyclic voltammograms (scan rate 100 mVs^{-1}) for a (A1) 25, (A2) 50, and (A3) 125 μm diameter copper microelectrode with different amounts of PIM-EA-TB deposited and immersed in 0.5 M NaCl. Inset showing the molecular structure of PIM-EA-TB. (B) Linear sweep voltammograms (scan rate 5 mVs^{-1}) for a (B1) 25, (B2) 50, and (B3) 125 μm diameter copper microelectrode without/with 4.0 μg μL^{-1} PIM-EA-TB coating immersed in 0.5 M NaCl(aq).

transport either by Cu^{+} or by Cl^{-} through the blocking CuCl film (or via grain boundaries). There is no chemical change at the copper surface associated with this process and an increase in driving force (potential) can be seen to increase the current in a close to Ohmic manner possibly due to ionic resistance across the CuCl layer.

Domain II: Beyond the onset of stochastic current fluctuations formation of Cu(II) at the copper surface may be possible and this causes a chemical change locally below the CuCl layer. Ionic transport through the CuCl layer could change and be associated with proton or Cu^{2+} mobility as well as with Cl^{-} uptake. Mechanical instability then causes breaking up of parts of the deposit and loss of particulate CuCl into the electrolyte solution.

The conditions at the copper electrode surface during domain II reactions are complex and will require further investigation. The Cu(II) species has not been identified and indeed there could be potential dependent changes in the chemical nature of the process. The peak feature at approximately 1.0 V *vs.* SCE is commonly observed underneath the stochastic current responses (even with

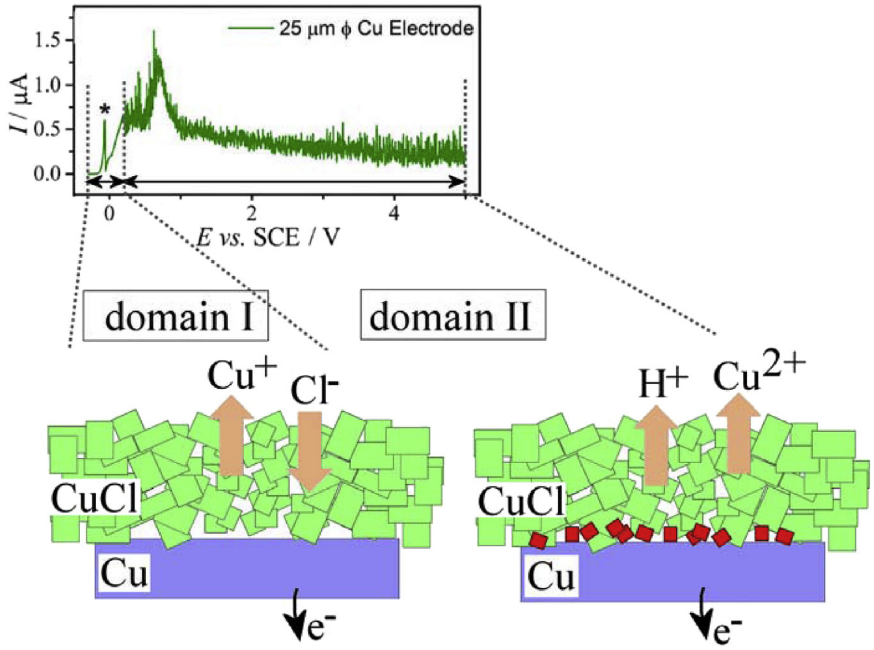

Fig. 11. Schematic drawing of the surface redox processes associated with domain I (at lower applied potential) and domain II (at higher applied potential) and the corresponding ion transport processes in the CuCl blocking layer.

PIM-EA-TB deposited) and this may imply further changes in surface chemistry with increased potential.

4. Conclusions and future work

It has been shown that complex stochastic current responses are observed at copper microelectrodes immersed in 0.5 M NaCl. In contrast to the previously (in more acidic media) usually assigned dissolution – precipitation type mechanisms [8], here a mechanism based on Cu(II) intermediates destabilizing the initially formed CuCl film is suggested. Both molecular scale dissolution (into ions) and break-up into particular CuCl colloid occurs in parallel. The latter particulate corrosion process is shown to be (at least in part) suppressed by coating microporous PIM-EA-TB over the copper surface. A mechanistic switch between potential domain I and potential domain II has been proposed due to Cu(II) being formed to account for some of the observed phenomena.

It is interesting to ask whether the non-stochastic oscillatory reactivity of copper in acidic chloride solution [6] is indeed purely due to the dissolution – precipitation reactions or whether underlying Cu(II) formation (as suggested previously [9,10]) may also account for the onset and dynamics observed in these processes. Preliminary data at microelectrodes reported here support this hypothesis. Further work including microelectrode studies in more acidic solution environment will be necessary and better *in situ* experimental tools identifying the reaction intermediates at the copper electrode | salt film interface will be desirable.

References

[1] L. Nunez, E. Reguera, F. Corvo, E. Gonzalez, C. Vazquez, Corrosion of copper in seawater and its aerosols in a tropical island, Curr. Sci. 47 (2005) 461–484.
[2] G. Kear, B.D. Barker, F.C. Walsh, Electrochemical corrosion of unalloyed copper in chloride media - a critical review, Curr. Sci. 46 (2004) 109–135.
[3] A. Zarrouk, I. Warad, B. Hammouti, A. Dafali, S.S. Al-Deyab, N. Benchat, The effect of temperature on the corrosion of Cu/HNO_3 in the presence of organic inhibitor: Part-2, Int. J. Electrochem. Sci. 5 (2010) 1516–1526.
[4] F. Arjmand, A. Adriaens, Influence of pH and chloride concentration on the corrosion behavior of unalloyed copper in NaCl solution: a comparative study between the micro and macro scales, Materials 5 (2012) 2439–2464.
[5] F. Mansfeld, G. Liu, H. Xiao, C.H. Tsai, B.J. Little, The corrosion behavior of copper-alloys, stainless-steels and titanium in seawater, Curr. Sci. 36 (1994) 2063–2095.
[6] M. Orlick (Ed.), Self-organization in Electrochemical Systems I, Springer, 2012, pp. 425–511.
[7] H.P. Lee, K. Nobe, A.J. Pearlstein, Film formation and current oscillations in the electrodissolution of Cu in acidic chloride media.1. Experimental studies, J. Electrochem. Soc. 132 (1985) 1031–1037.
[8] A.J. Pearlstein, H.P. Lee, K. Nobe, Film formation and current oscillations in the electrodissolution of copper in acidic chloride media. 2. Mathematical-model, J. Electrochem. Soc. 132 (1985) 2159–2165.
[9] F.K. Crundwell, The anodic-dissolution of copper in hydrochloric-acid solutions, Electrochim. Acta 37 (1992) 2707–2714.
[10] M. Itagaki, T. Mori, K. Watanabe, Channel flow double electrode study on electrochemical oscillation during copper dissolution in acidic chloride solution, Curr. Sci. 41 (1999) 1955–1970.
[11] Y.X. Jia, A. Bi, A. Selimovic, R.S. Martin, I.Z. Kiss, Periodic and complex waveform current oscillations of copper electrodissolution in phosphoric acid in an epoxy-based microchip flow cell, J. Solid State Electrochem. 19 (2015) 3241–3251.
[12] R.J. Forster, Microelectrodes – new dimensions in electrochemistry, Chem. Soc. Rev. 23 (1994) 289–297.
[13] A.M. Bond, Past, present and future contributions of microlectrodes to analytical studies employing voltammetric detection – a review, Analyst 119 (1994) R1–R21.
[14] D.R. Lide (Ed.), CRC Handbook of Chemistry and Physics, 74th edition, CRC Press, London, 1993-1994, pp. 8–49.
[15] M.Yu. Skripkin, L.V. Chernykh, L.V. Stepakova, V.A. Samokhvalova, Effect of alkali metal chlorides on the solubility in ternary water salt systems containing copper monochloride, Russ. J. Appl. Chem. 75 (2002) 1051–1054.
[16] P.M. Budd, B.S. Ghanem, S. Makhseed, N.B. McKeown, K.J. Msayib, C.E. Tattershall, Polymers of intrinsic microporosity (PIMs): robust, solution-processable, organic nanoporous materials, Chem. Commun. (2004) 230–231.
[17] T.O. McDonald, R. Akhtar, C.H. Lau, T. Ratvijitvech, G. Cheng, R. Clowes, D.J. Adams, T. Hasell, A.I. Cooper, Using intermolecular interactions to cross-link PIM-1 and modify its gas sorption properties, J. Mater. Chem. A 3 (2015) 4855–4864.
[18] N.B. McKeown, P.M. Budd, Exploitation of intrinsic microporosity in polymer-based materials, Macromolecules 43 (2010) 5163–5176.
[19] F.J. Xia, M. Pan, S.C. Mu, R. Malpass-Evans, M. Carta, N.B. McKeown, G.A. Attard, A. Brew, D.J. Morgan, F. Marken, Polymers of intrinsic microporosity in electrocatalysis: novel pore rigidity effects and lamella palladium growth, Electrochim. Acta 128 (2014) 3–9.
[20] D.P. He, Y.Y. Rong, Z.K. Kou, S.C. Mu, T. Peng, R. Malpass-Evans, M. Carta, N.B. McKeown, F. Marken, Intrinsically microporous polymer slows down fuel

cell catalyst corrosion, Electrochem. Commun. 59 (2015) 72–76.
[21] Y.Y. Rong, R. Malpass-Evans, M. Carta, N.B. McKeown, G.A. Attard, F. Marken, Intrinsically porous polymer protects catalytic gold particles for enzymeless glucose oxidation, Electroanalysis 26 (2014) 904–909.
[22] M. Carta, R. Malpass-Evans, M. Croad, Y. Rogan, J.C. Jansen, P. Bernardo, F. Bazzarelli, N.B. McKeown, An efficient polymer molecular sieve for membrane gas separations, Science 339 (2013) 303–307.
[23] E. Madrid, Y.Y. Rong, M. Carta, N.B. McKeown, R. Malpass-Evans, G.A. Attard, T.J. Clarke, S.H. Taylor, Y.T. Long, F. Marken, Metastable ionic diodes derived from an amine-based polymer of intrinsic microporosity, Angew. Chem. Int. Ed. 53 (2014) 10751–10754.
[24] J.J. Fritz, Representation of the solubility of CuCl in solutions of various aqueous chlorides, J. Phys. Chem. 85 (1981) 890–894.
[25] D.R. Lide (Ed.), CRC Handbook of Chemistry and Physics, 74th edition, CRC Press, London, 1993-1994, pp. 4–149.
[26] A.V. Benedetti, P.T.A. Sumodjo, K. Nobe, P.L. Cabot, W.G. Proud, Electrochemical studies of copper, copper-aluminium and copper-aluminium-sliver alloys: impedance results in 0.5 M NaCl, Electrochim. Acta 40 (1995) 2657–2668.
[27] D.R. Lide (Ed.), CRC Handbook of Chemistry and Physics, 74th edition, CRC Press, London, 1993-1994, pp. 4–141.
[28] B. Yin, S. Zhang, X. Zheng, F. Qu, X. Wu, Cuprous chloride nanocubes grown on copper foil for pseudocapacitor electrodes, Nano Micro Lett. 6 (2014) 340–346.
[29] P.M. Budd, B.S. Ghanem, S. Makhseed, N.B. Mckeown, K.J. Msayib, C.E. Tattershall, Polymers of intrinsic microporosity (PIMs): robust, solution-processable organic nanoporous materials, Chem. Commun. (2004) 230–231.